JAERI-M
5929

TWO-STAGE ACCELERATION OF AN ION BEAM FOR POWERFUL INJECTORS

December 1974

Yoshihiro OHARA and Tohru SUGAWARA*

日本原子力研究所
Japan Atomic Energy Research Institute

JAERI - M 5929

Two-Stage Acceleration of an Ion Beam for Powerful Injectors

Yoshihiro OHARA and Tohru SUGAWARA*

Thermonuclear Fusion Laboratory, Tokai, JAERI

(Received November 25, 1974)

The beam divergence in a two-stage ion source has been studied by calculating the beam trajectories in the space-change-limited flow. The second stage consists of the single aperture exit electrode and the spherically concave electrode as the emitter of a homogeneous beam with initial energy. Optimum configurations of the electrodes to give a low divergence beam were obtained for the aspect ratios of 1 and 2/3, the energy ratios of 1/3 and 1/2, and the normalized perveances of 0.6 to 1.5. The beam divergence increases rapidly with the perveance beyond a certain critical value. The increment of the final beam divergence due to the first stage divergence is equal to the beam divergence in the first stage.

---

* On leave from the Research and Development Center, Tokyo Shibaura Electric Co. Ltd., Kawasaki.

JAERI−M 5929

大容量粒子入射装置のための イオンビームの2段加速

日本原子力研究所東海研究所核融合研究室

小原祥裕，菅原　亨*

（1974年11月25日受理）

空間電荷制限電流状態のもとでのビーム軌道を計算することによって，インジェクタ用二段加速イオン源のビームの発散を調べ，その設計を試みた。第2段加速部は，初速をもった発散性ビームが均一に放出される球面状多孔形電極及び単一孔引出し電極より構成される。アスペクト比（電極孔半径／引出し電極間隔）が1及び⅔，エネルギー比（第1段加速エネルギー／最終ビームエネルギー）が⅓と½，規格化パービアンスが0.6～1.5について，電極の最適構造が求められた。パービアンスがある値より大きくなると，ビームの発散は急に増大し，他のパラメータによって補償することが困難となる。又，第1段目の発散はそのまま第2段目の発散に加えられることがわかった。

* 外来研究員（東京芝浦電気株式会社　総合研究所）

目　次　な　し

§1. Introduction

The neutral beam injection is one of the most powerful and effective methods for heating a tokamak plasma, which has been confirmed in ATC[1], OHMAK[2] and CLEO[3] experiments. The neutral beam with tens of kilovolts energies is now achieved[4),5)]. At the same time, however, developments of more powerful injectors are desired for the next generation tokamaks. Moreover the increase of target plasma thickness demands the further raise of beam energy. For future tokamaks such as JT-60, JET or F/BX, the neutral beam injectors require the beam with energy of 50 ~100 keV, equivalent beam current of 20~30A and divergence within one degree. However, if the ion source has a configuration of one stage acceleration, the decrease of beam power flux density is inevitable with the increase of acceleration energies above some level because of the electrical breakdown problems. In fact, the breakdown distance for vacuum gaps is practically proportional to the square of an applied voltage[6] and the ion current density is space-charge-limited. Consequently, the power flux density may decrease inversely as three-halves power of the acceleration voltage, when the gap distance is chosen according to the breakdown distance. This restriction is released by decoupling the current extraction stage and the acceleration stage, i.e., by employing a multiple stage acceleration system. In the first stage, namely, the current extraction stage, the configuration with gap distances of several millimeters and electric fields of several kV/mm adopted in this paper are similar to those which have been successfully operated at ORNL[4], CLM[7], LBL[5], etc.. The purpose of this paper is to investigate optimum electrode geometries of the second stage for low beam divergence which have not been studied quantitatively so far.

§2. Electrode Geometry

The two stage acceleration system has four electrodes. The first stage is composed of the first and second electrode, and the second stage is composed of the second, third and fourth electrode. The configuration of the second stage is assumed

axisymmetric and is shown in Fig. 1. The first electrode in contact with a source plasma is multi-aperture type and is held at the positive high potential corresponding to the desired beam energy. The second electrode is also multi-aperture type and spherically concave. It is assumed that the radius of each aperture is small enough compared with the radius of the electrode. Therefore, the spherical surface would be regarded as equipotential since the immersion of field from the first stage may be neglected. Further we assume from the surface the ion beam is emitted uniformly to the normal direction with the initial energy E_f and divergence ω_f. The beam forming edge of this electrode is not taken into account, because effects of the edge shapes on the beam formation become weaker with the increase of initial energies. The third electrode is a single disk aperture and is biased at negative voltage to suppress the electron backstreaming from the subsequent beam-plasma region. The fourth electrode is also single aperture and is grounded electrically. It may be natural to regard the zero potential surface in contact with this electrode as the boundary between the ion sheath and beam-plasma. The beam-plasma is produced by collision between the primary beam ion and the residual neutral gas. In the beam-plasma region, the ion beam is not exposed to the space charge expansion[6]. Accordingly, the beam divergence is defined on this boundary surface. The ion extraction from the beam-plasma region is ignored.

Effects of the angular distribution breadth of the beam from the first stage is considered as follows. The beam is emitted in the three directions from the equipotential surface at the second electrode, namely, the normal direction to the electrode and the divergent and convergent directions at an angle of ω_f (Fig. 1). Each direction are equally weighted.

§3. Computational Method[8),9)]

Trajectories of ion beam are calculated by the equations of space-charge-limited current flow. The equations for space-charge-limited current are

Poisson's equation $\nabla^2\phi = -\rho/\varepsilon_0$ (1)

Equation of motion $m\,d\vec{v}/dt = e\vec{E}$ (2)

Equation of continuity $\nabla\cdot\vec{J} = \nabla\cdot(\rho\vec{v}) = 0$ (3)

where rationalized mks units are used and the notations have usual meanings. The magnetic field in the extraction region has bad effects on beam optics and produces separation of ion species, H_1^+, H_2^+, H_3^+, etc.. Therefore, the magnetic field free ion source is adopted for the present case. On the other hand, the magnetic field produced by ion beam itself is negligible. Hence the magnetic field is not taken into account in the equation (2). Under these conditions, it is easy to verify that beam trajectories don't depend on mass and electric charge. Historically, analytic solutions to these equations have been formulated by Langmuir and Blodgett for plane parallel, coaxial cylindrical and coaxial spherical electrodes. More complicated geometries have proved intractable to analytic solution, but they can be solved by numerical methods.

A block diagram of the digital computer program is shown in Fig. 2. First, data are read in to define the dimensions of the problem, the electrode configuration, the electrode potentials, the total current and other parameters needed for solution. The second acceleration region is divided into 30(radially)× 50(axially) meshes. Next, the Poisson's equation is solved to provide the potential distribution by means of successive over relaxation method. For the cylindrical coordinates, the finite difference equation at $R=r_0$ $(\neq 0)$ is given by

$$b_1\phi_A + b_2\phi_B + b_3\phi_C + b_4\phi_D + b_5\phi_o = -\rho/\varepsilon_0, \qquad (4)$$

where

$$b_1 = 2/a_1(1+a_1)h_1^2$$

$$b_2 = (2r_0+h_2)/r_0a_2(1+a_2)h_2^2$$

$$b_3 = 2/(1+a_1)h_1^2$$

$$b_4 = (2r_0-a_2h_2)/r_0(1+a_2)h_2^2$$

$$b_5 = -2/a_1h_1^2 - 2/a_2h_2^2 - (1-a_2)/r_0a_2h_2.$$

On the axis, Eq. (4) is replaced by

$$b_1\phi_A + b_6\phi_B + b_3\phi_C + b_7\phi_D = -\rho/\varepsilon_0 , \tag{5}$$

where

$$b_6 = 4/a_2^2h_2^2$$

$$b_7 = -2/a_1h_1^2 - 4/a_2^2h_2^2 .$$

ϕ_A, ϕ_B, ϕ_C, ϕ_D, ϕ_0 are the potentials at points A, B, C, D and O respectively; r_0, h_1, h_2, a_1, a_2 are defined in Fig. 3. The electric field is obtained by linear interpolation of the mesh values. After the field distribution is obtained, twenty beam trajectories are then calculated to provide a space charge distribution. The space charge density in the mesh ρ_{ij} is

$$\rho_{ij} = \frac{1}{V_{ij}} \sum_m I^{(m)} t_{ij}^{(m)} , \tag{6}$$

where V_{ij} is the volume of torus whose cross section is (i,j) cell, $I^{(m)}$ is the total current in the m-th beam and $t_{ij}^{(m)}$ is the time interval in which the m-th beam passes through the (i,j) cell. This is used in turn for a new solution of Poisson's equation followed by a re-computation of the trajectories. The calculation is thus repeated until the beam trajectories converge to a solution.

The validity of the program is checked by changing the potential, current density and dimensions in a fashion that keeps the perveance constant. The beam energy has 1 ~ 2 percent error because of the finite mesh approximation, but no significant change in the trajectories occurred.

§4. Method of Optimum Parameter Survey

When the space-charge-limited current is extracted from the source plasma, the meniscus of a plasma surface depends on the aspect ratio of the first stage which is defined by the ratio of the first stage aperture radius to the distance between the first and second electrode. It is known that the aspect ratio should be less than 0.5 in order to obtain the low divergence

beam[6]. In the initial acceleration, the multiple aperture configuration with a high transparency is to be employed for the intense beam. However, since the second stage acceleration region is separated from the source plasma, the aspect ratio of the second stage can be chosen arbitrarily. The interception current on the third electrode per unit beam current decreases with the increase of the third aperture radius. Consequently, we consider the configuration where the single aperture of the third electrode contains the beam from many apertures of the second electrode.

Fundamental quantities for the second stage design are the perveance ($G = I/V_p^{3/2}$, where I and V_p are the beam current per aperture and the voltage applied to the first electrode respectively), the ratio of the initial acceleration energy to the final beam energy(f), and the aspect ratio($S = R_1/D_1$, where R_1 is the emitting surface radius, and D_1 the distance between the second and the third electrode, respectively). When the aspect ratio is too small for a fixed value of potential, the electric field is so weak that it may produce the electrical potential hill along the beam trajectories and hence it may enhance the beam divergence. On the other hand, the aberration of lens becomes severe, as the aspect ratio is greater than 1.0. Therefore, the geometries with the aspect ratios of 1 and 2/3 are adopted. The condition for the potential to decrease monotonically is

$$G/k \leq \frac{4\pi}{9} S^2(1-\sqrt{f})(1+2\sqrt{f})^2 , \qquad (7)$$

in the plane diode approximation, where the perveance constant k is given by $\varepsilon_0\sqrt{2e/M}$ and is equal to 0.12256 micropervs. for proton. Hereafter, G/k is called the normalized perveance. The derivation is shown in Appendix I. The right hand side of Eq. (7) takes the maximum value at f = 1/4, but here f is taken as 1/2 and 1/3, where corresponding second acceleration energy is equal to and greater than the first one, respectively.

Moreover, the potential has to be negative under the third electrode. Taking account of only the potential difference between the edge and axis of the beam due to the space charges,

the following condition must be fulfilled on the applied negative voltage (V_N);

$$|V_N|/V_p > G/4\pi k \ . \qquad (8)$$

A large negative voltage (V_N) is undesirable, because the secondary electrons emitted from the third electrode are accelerated to bombard the second electrode and the heat load of the electrodes increases. From Eqs. (7) and (8), a range of G/k is chosen to be around one.

There are more than ten parameters which characterizes the second stage, namely, G, V_p, V_N, f, s, a, Ψ, ω_f, mass, electric charge, etc.. This makes it necessary to simplify the procedure of seeking for the optimum parameters. At first, following conditions are assumed. We consider proton beam H^+ with V_p = 75kV, R_1 = 5 cm, $R_2 = R_3$ and R_2/D_2 = 3/2. The ratio $R_2/D_2 = 3/2 \backsim \pi/2$ is derived by the fact that the external field penetrates through an aperture roughly in the length of (aperture diameter)/π. It is known that the gap length between the third and fourth electrode should be kept short for low divergence beam[6]. In the present work, as an example, the gap length D_3 is chosen $0.2D_1$. The grounded electrode is so thick that the beam-plasma boundary is connected to the inside surface of the electrode hole. Here, the thickness D_4 is chosen to be equal to D_3.

Further we assume the energy ratio f, aspect ratio s and aperture ratio a(= R_2/R_1). Under these conditions, the optimum convergence angle Ψ of the emitter and the potential of negative electrode V_N are surveyed which give the maximum extractable beam current. By the "optimum" parameters we mean that

(1) the divergence of all the beamlets are within one degree,

(2) the potential at the saddle point on the Z-axis is slightly negative, that is, about -1kV.

This procedure is repeated changing a set of values f, s and a. Following cases are surveyed ; (A) f = 1/2, s = 2/3, (B) f = 1/3, s = 2/3, (C) f = 1/2, s = 1/1 and (D) f = 1/3, s = 1/1. The flow chart is shown in Fig. 4.

§5. Results

Firstly, the angular divergence for $\omega_f = 0$ is examined, where all the beam elements are emitted normally to the second electrode. The emittance diagram at the beam-plasma boundary is shown in Fig. 5. The behaviour of the beam divergence at the beam-plasma surface is that the peripheral beam is convergent compared with the slightly inner beam. The emittance diagram changes in shape as is also shown in the same figure with the increase of perveance. The divergence of each beamlet increases almost proportionally to the perveance. In the case of I = 3.5 A, the beam can pass through the cylindrical drift tube which is 5 m long and 30 cm in radius, where the acceptance diagram of the cylinder is also shown by broken lines. However, in other cases, a part of the beam hits the drift tube surface. After all, there exists an optimum current in a fixed structure, but the value permits only small error within several percent. Therefore, it is very important to produce a stable source plasma.

Figure 6 shows the dependence of the beam divergence on the convergence angle Ψ. When the normalized perveance G/k is 0.6(a), Ψ has an optimum value. But, when the perveance becomes greater than 1.0 (b), the divergence cannot be made smaller than one degree for any values of Ψ. In the case of (a), the error in Ψ must be less than one percent. Therefore, the attention must be paid to the misalignment of the electrodes and the deformation due to the thermal stress.

In the next place, the dependence of the beam divergence on the exit aperture radius is examined for each perveance by matching the angle Ψ with the lens action. The large aberration appeares as shown in Fig. 7, when the beam edge is close to the third electrode or when the aperture radius becomes large. In the former case, the beam occupies not only the central region of the lens of saddle-like potential but also the region of the extremely crooked equipotential lines near the electrode edge. In the latter case, the distortion of the field due to the hole reaches close to the second electrode.

Using the optimized values of Ψ and a, the relation between the beam divergence and perveance is obtained as plotted in

Fig. 8(a). It is noted that the beam divergence increases rapidly with the perveance above a certain value, which depends on S and f. Figure 8(b) shows the optimum lines for each case (A), (B), (C), and (D). The points plotted indicate the convergence angle Ψ which give the maximum beam current for a fixed aperture ratio a. The following remarks can be concluded from Fig. 8.

(1) When the second stage is of the single aperture type, it is difficult to obtain 75 KeV ion beams whose currents exceed 3A.

(2) The beam current is not proportional to S^2 but to S roughly.

(3) The beam current increases above 10 ~ 20% with the increase of the energy ratio f.

Beam trajectories in the case of a = 1.0 are shown in Fig. 9, where the total beam current is 3A and f is 1/3. Current density at the emitting surface is 35.4 mA/cm^2, and the potential at the saddle point under the negative electrode is -1.0 kV. The beam divergences under these conditions are within ± 0.64 degree.

In order to get more powerful ion source, we consider an electrode structure composed of seven apertures as shown in Fig. 10, where each aperture is scaled down to 3/10 of the above example. Then, the beam current of 21A can be expected from the emitting surface having the same area as the above case. The beam current density at the emitting surface this time becomes 393 mA/cm^2, which has been obtained experimentally at ORNL, LBL, CLM, etc. The spacing between the second and third electrode is reduced to 1.5 cm from 5.0 cm, and the voltage of 73 kV is applied between these electrodes. However, the voltage is still smaller than the breakdown voltage estimated from the empirical formula. The interaction among the neighboring beams can be neglected, which is plausible by the equipotential line shown in Fig. 9. Thus, it would be possible to obtain the beam power density about 20 kW/cm^2 with the total beam current about 20 ~ 30 A.

Secondly, the effects of initial beam divergence ω_f is examined for the above optimum geometries. The focal length of the exit lens is insensitive to the initial divergence in the range of $\omega_f <$ one degree, whereas the final beam divergence is strongly influenced. Figure 11 shows that the increment of the final beam divergence is uniform with respect to each beamlet and is equal ω_f. The same behaviour is seen for other sets of f, s, and G/k. For the present case, the value of $|\omega_f|$ must be less than 0.25 degree, and this is a very severe demand. But, there is an exceptional case where ω_f is permitted up to about 0.8 degree. Anyway, ω_f must be smaller than 1.0 degree.

This behaviour means that the transverse beam velocity is amplified during the passage through the second acceleration region. The motion of the ions in a given potential field (ϕ) is described as

$$\frac{d}{d\ell}\left(u \frac{dr}{d\ell}\right) = \left(\frac{\partial u}{\partial r}\right)_z \quad , \tag{9}$$

where r and z are the cylindrical coordinates, ℓ is the distance along the trajectory, and $u = \sqrt{1-\phi/V_p}$. By integrating along the beam trajectory (C), we obtain

$$\left(\frac{dr}{d\ell}\right)_b = \sqrt{f}\left(\frac{dr}{d\ell}\right)_f - \int_c d\ell \left(\frac{\partial u}{\partial r}\right)_z \, , \tag{10}$$

where the suffixes f and b denote the quantities at the emitting surface and at the beam-plasma surface, respectively. Consequently, for the small deviation of the emitting beam angle, the final beam divirgence decreases only by $\sqrt{f}$ times as large as the initial d vergence, if the contribution from the second term in the right hand side of Eq. (10) can be ignored. In our cases, however, the line integral is sensitive to the beam trajectory. Calculated behaviour of the ion beams is considered to arise from this effect. In order to reduce the sensitivity of the line integral to the trajectory, the configuration seems to require a fairly small convergence angle of the emitting surface. However, the heat load on the electrodes comes to the front in this case, because the beam current per one exit hole becomes small.

It is possible to improve the permissible divergence of the first stage ω_f as follows. Namely, it is assumed that the each beam element are not emitted to the normal direction from the second electrode but slightly to the oblique direction as shown in Fig. 12. Here, ω_i is the function of the beam element number. When ω_i has the distribution as shown in Fig. 13, allowable ω_f is improved from 0.25 degree to 0.5 degree for the present case. The control of ω_i within 2 degree is possible by displacing the axises of each aperture of the first and second electrode. This method can be applied to other cases.

§6. Conclusion

Beam divergences in the two stage acceleration are numerically examined for the above-mentioned second stage configuration, assuming the second electrode as a homogeneous beam emitting surface. The results are summarized as follows;

(1) The beam divergence increases rapidly with perveance above a certain perveance value.

(2) In the present configuration, it is difficult to obtain the total beam current more than 3 A, or power density more than 20 kW/cm^2.

(3) The increment of final beam divergence due to the initial divergence is equal to the initial one.

In the design of two stage sources, the aspect ratio S, acceleration ratio f, and normalized perveance G/k should be chosen according to Fig. 8 from the viewpoints of the breakdown and beam current density.

Acknowledgements

The authors are grateful to Drs. H. Shirakata and S. Matsuda for valuable discussions. Thanks are also due to Dr. S. Mori for his support and encouragement.

References

1) K. Bol et al.: Phys. Rev. Letters 32(1974) 661.
2) L. A. Berry et al.: Plasma Physics and Controlled Nuclear Fusion Research (Proc. 5-th Intern. Conf. Tokyo 1974) IAEA-CN-331/A5-2.
3) J. G. Cordey, et al.: CLM-P383, Feb.(1974).
4) W. L. Stirling et al.: Proc. 2-nd Inter. Conf. on Ion Sources, Vienna (1972).
5) W. R. Baker et al.: Proc. 5-th Symp. on Engineering Problems of Fusion Research, Princeton Univ., (1973).
6) J. R. Coupland et al.: Rev. Sci. Instrum. 44, 1258 (1973).
7) D. Aldcroft et al.: Proc. 3rd Inter. Symp. on Toroidal Plasma Confinement, B-24, Garching (1973).
8) D. G. Bate: CLM-R53, Jan. (1966).
9) J. L. Harrison: J. Appl. Phys. 39, 3827 (1968).

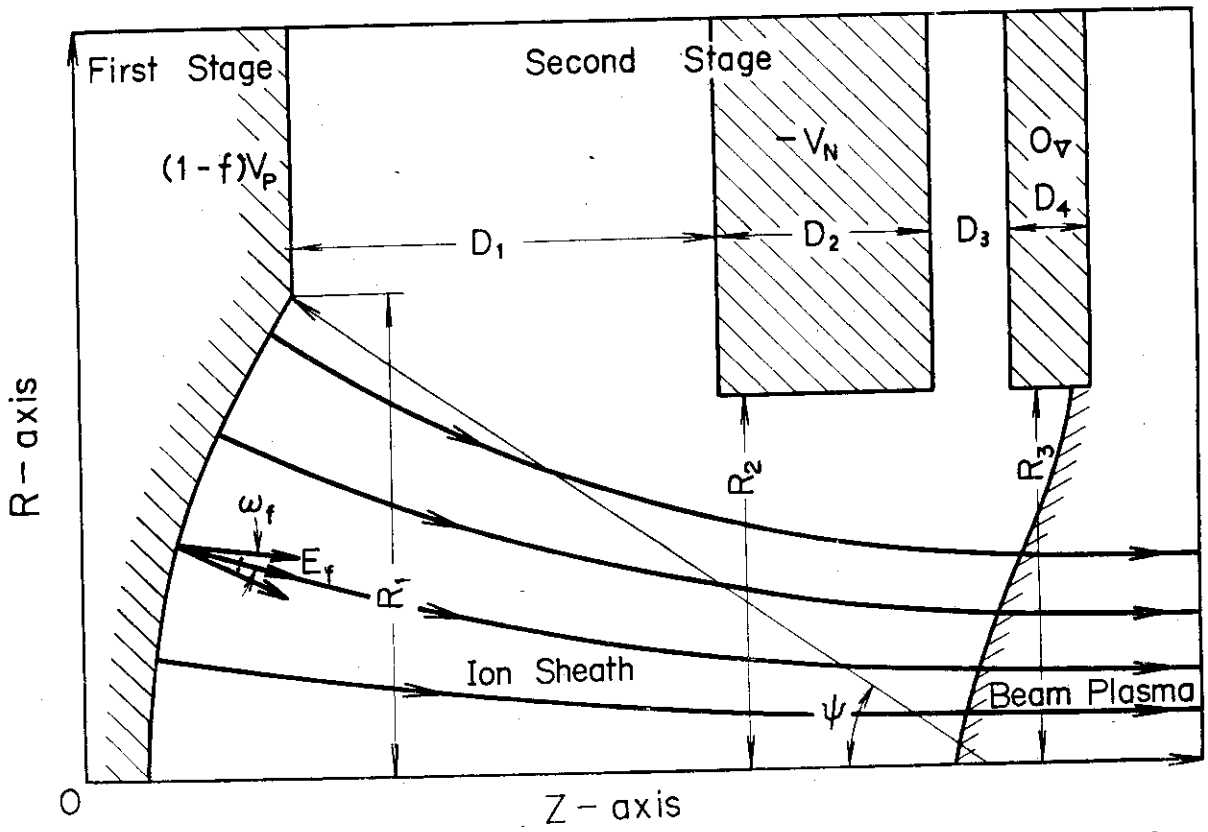

Fig. 1 Configuration of the second stage. The electrode on the left-hand side is the second electrode.

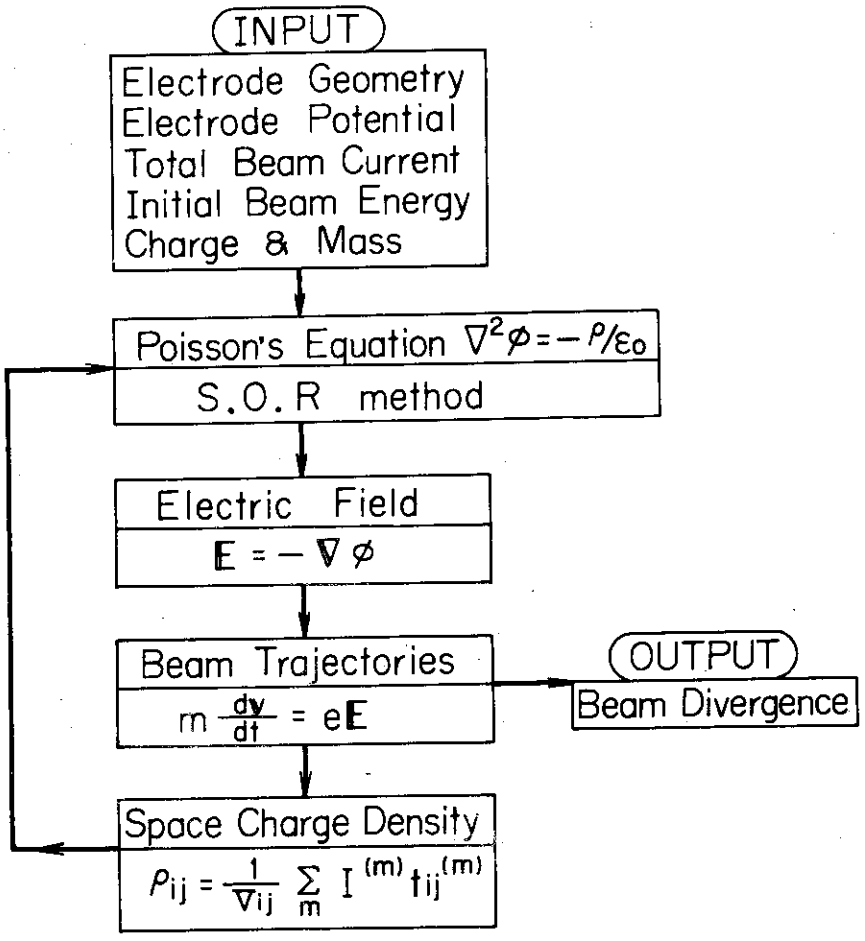

Fig. 2 Block diagram of computer program.

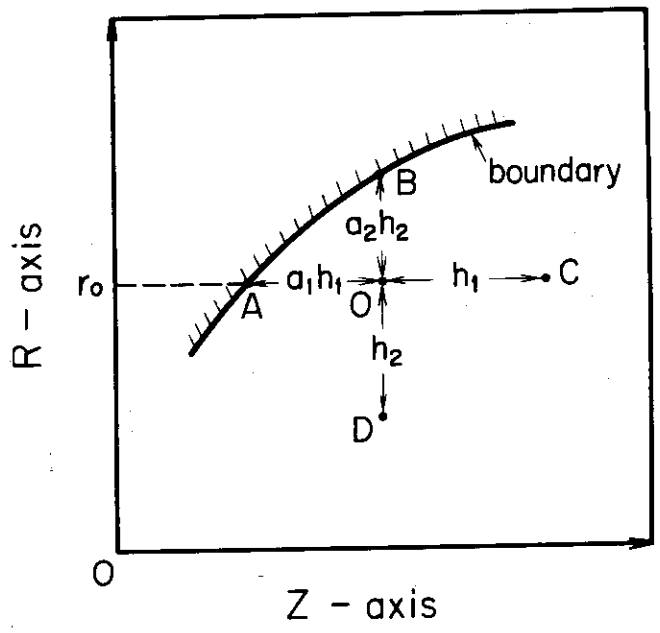

Fig. 3 Showing the relationship between the points A,B,C,D and O used in Eq.4.

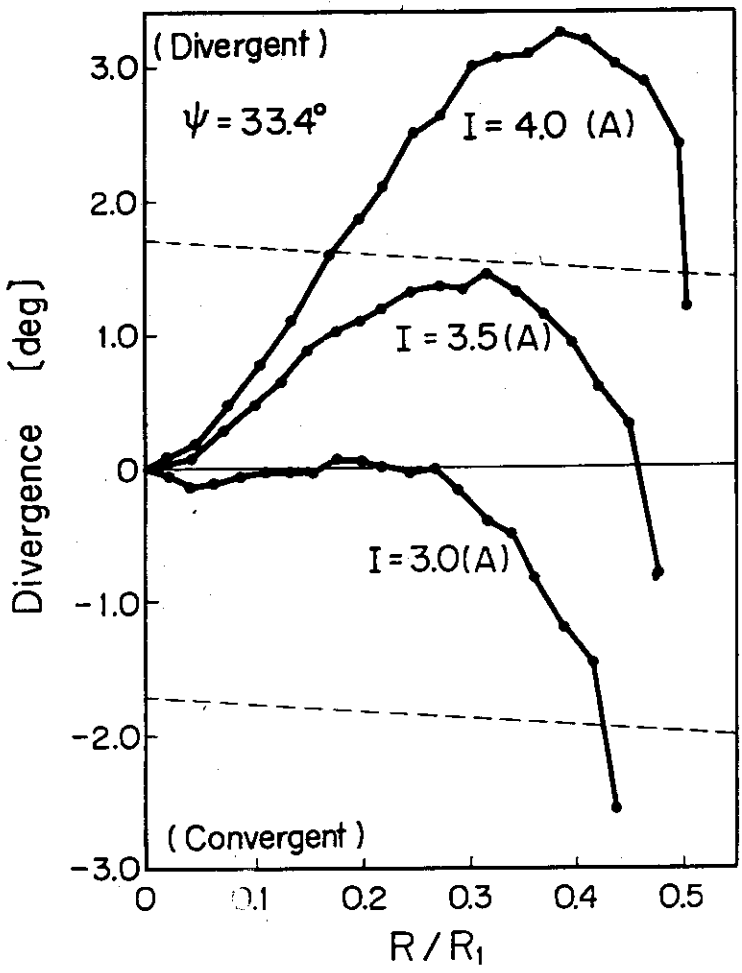

Fig. 5 Emittance diagram at the beam-plasma boundary; f=1/3, s=1, a=0.6, ψ=33.4 degree, I=3.0A, 3.5A and 4.0A. The broken line indicates the acceptance diagram of the drift tube of 5m long and 30cm in radius.

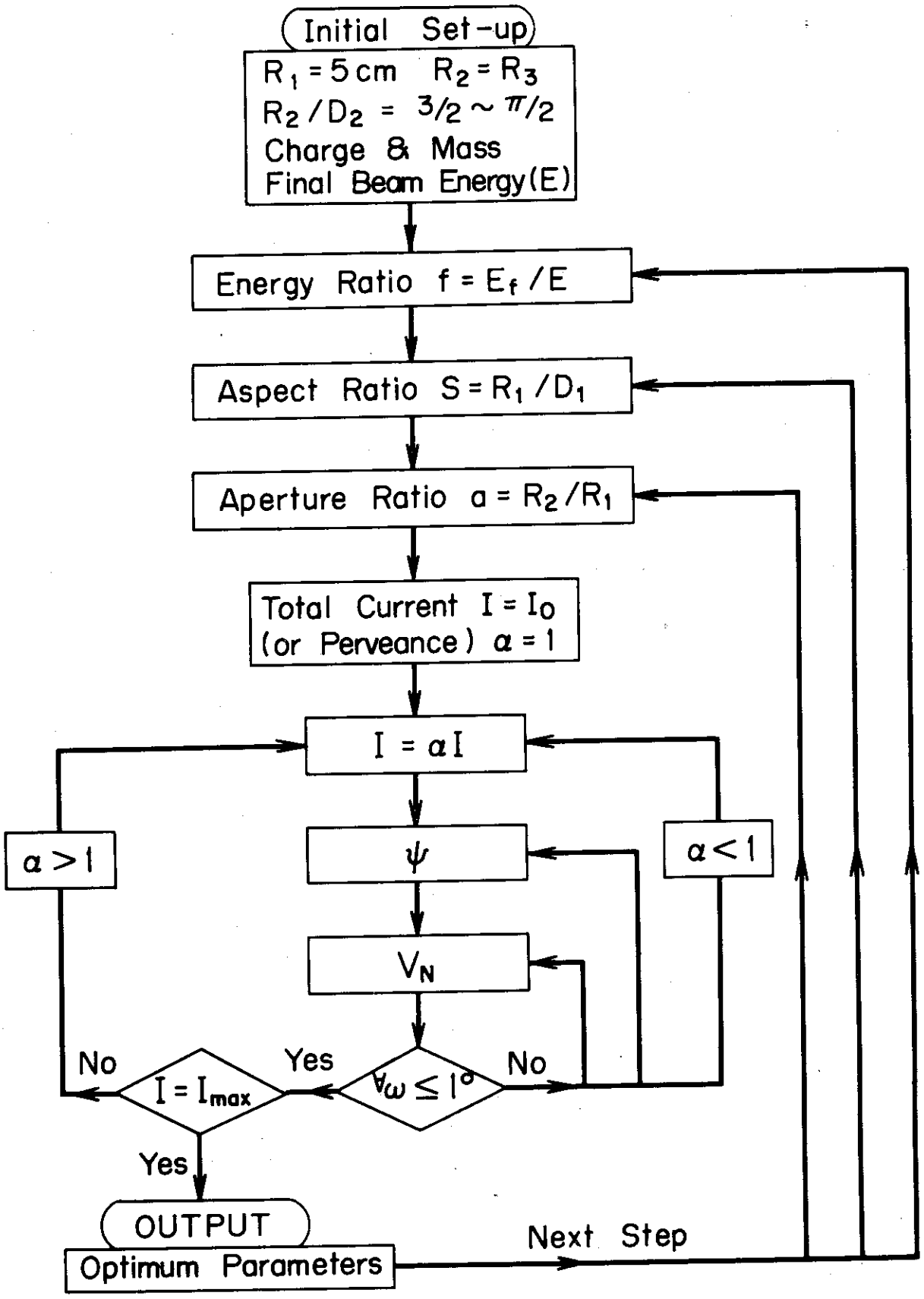

Fig. 4 Flow chart for the optimum parameter survey.

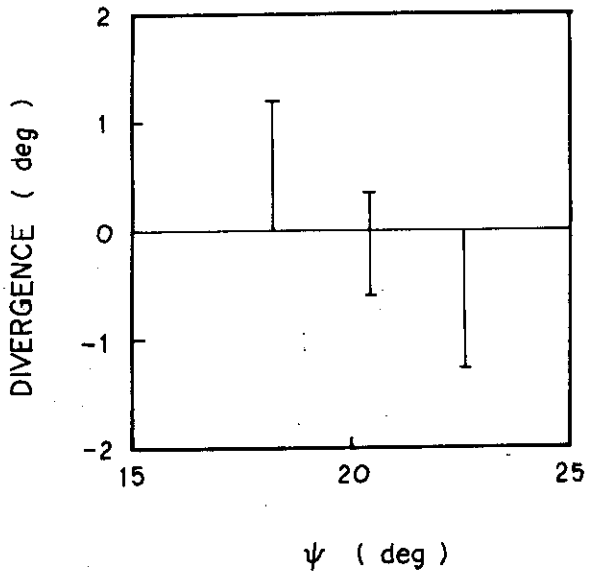

Fig. 6(a) Dependence of the beam divergence on the convergence angle of the emitting surface; f=1/3, s=2/3, G/R=0.6, a=0.7

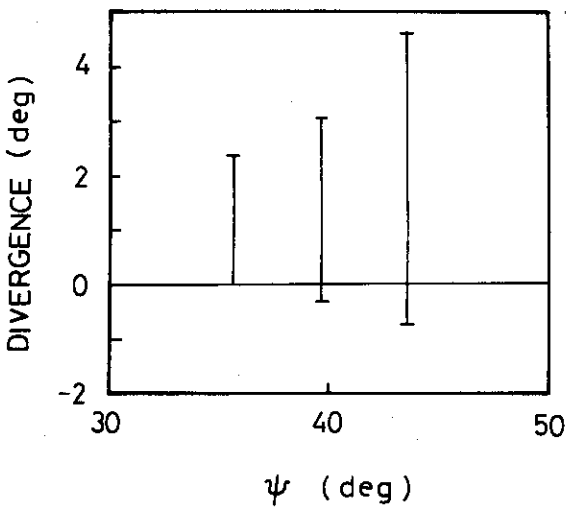

Fig. 6(b) Dependence of the beam divergence on the convergence angle of the emitting surface; f=1/3, s=2/3, G/k= . , a=0.6.

Fig. 6 Dependence of the beam divergence on the convergence angle of the emitting surface; (a) f=1/3, s=2/3, G/k=0.6, a=0.7, (b) f=1/3, s=2/3, G/k=1.0, a=0.6.

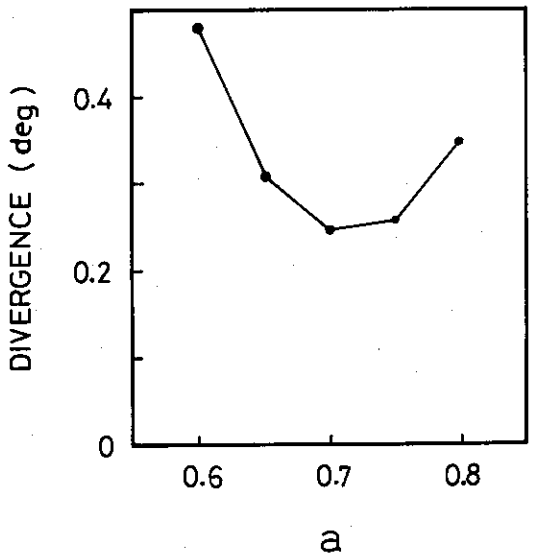

Fig. 7 Beam divergence versus exit hole radius for f=1/3, s=2/3 and G/k=0.6.

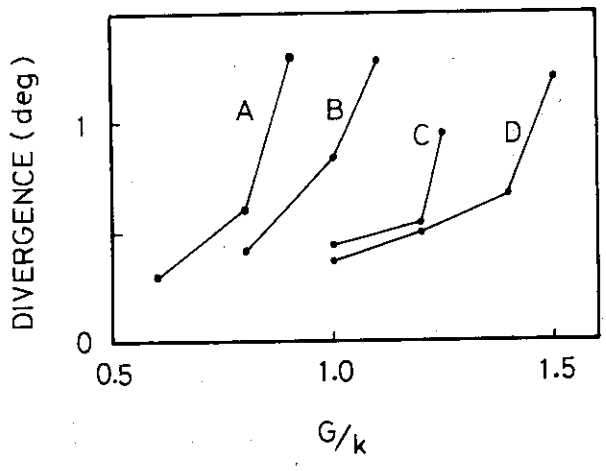

Fig. 8(a) Optimum values of the convergence angle and exit hole radius; (A) f=1/3, s=2/3, (B) f=1/2, s=2/3, (C) f=1/3, s=1, (D) f=1/2, s=1.

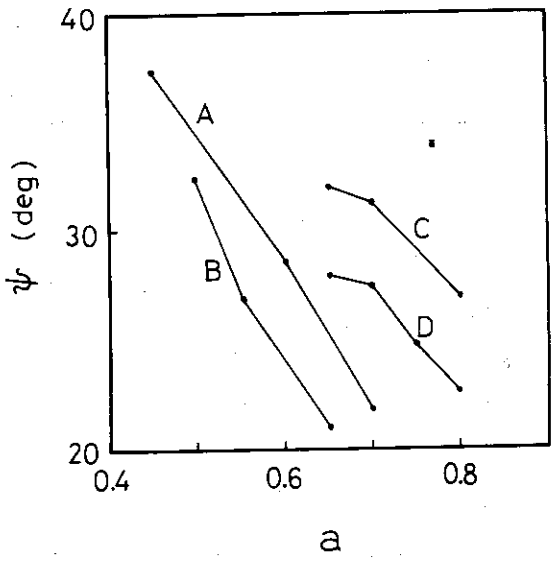

Fig. 8(b) The relation between the beam divergence and the perveance; (A) f=1/3, s=2/3, (B) f=1/2, s=2/3, (C) f=1/3, s=1, (D) f=1/2, s=1.

Fig. 8 Optimum values of the convergence angle and exit hole radius (a), and the relation between the beam divergence and the perveance (b); (A) f=1/3, s=2/3, (B) f=1/2, s=2/3, (C) f=1/3, s=1, (D) f=1/2, s=1.

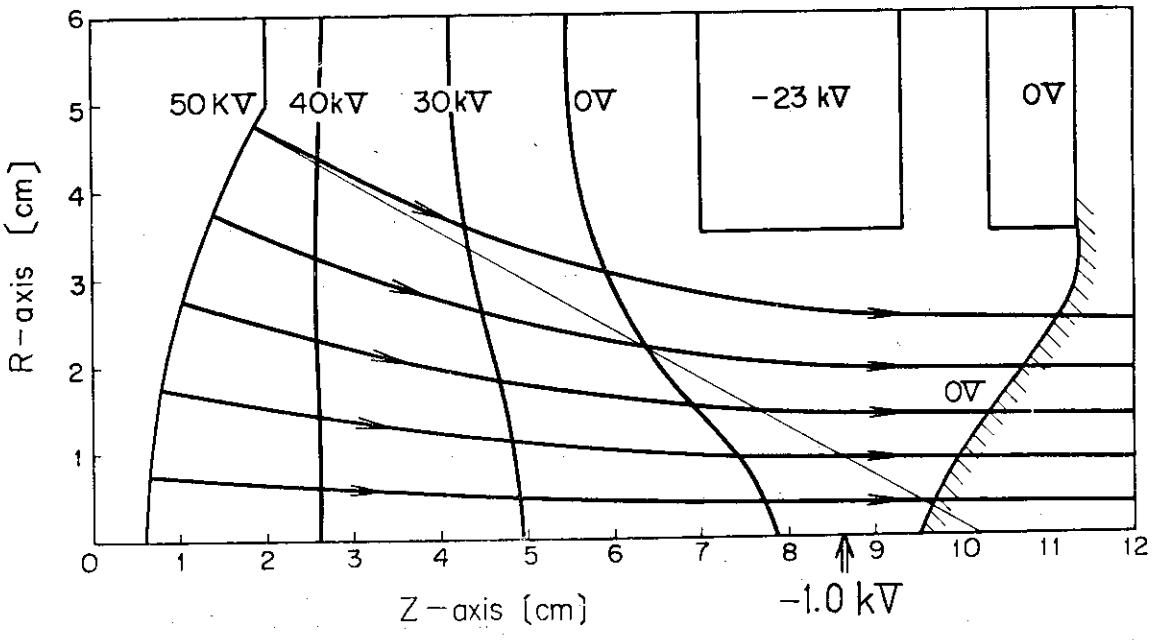

Fig. 9 A typical example of the optimum configuration and the beam trajectories; f=1/3, s=1, a=0.7, G/k=1.192 (total current of 3.0A), Ψ=31.3 degree.

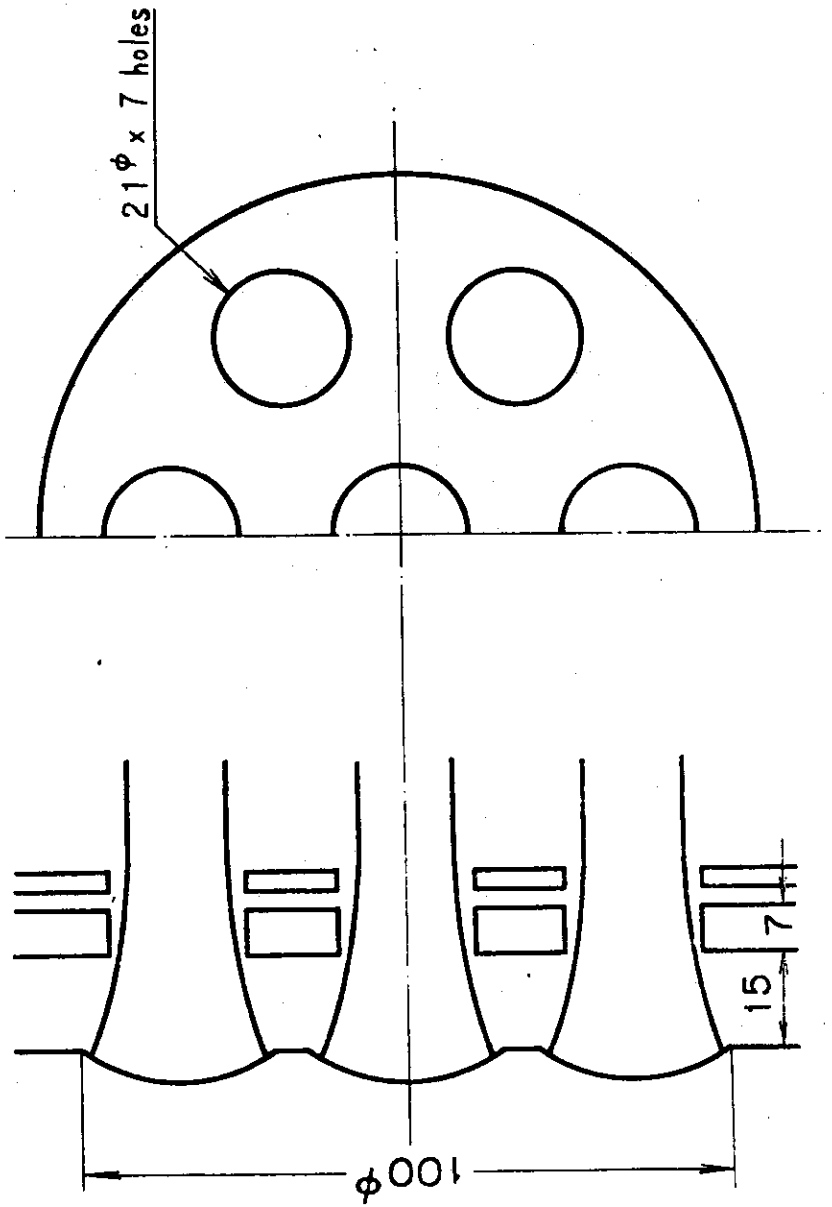

Fig. 10 One of the second stage configurations; f=1/3, s=1, a=0.7, G/k=8.342 (total current of 21A), Ψ=31.3 degree.

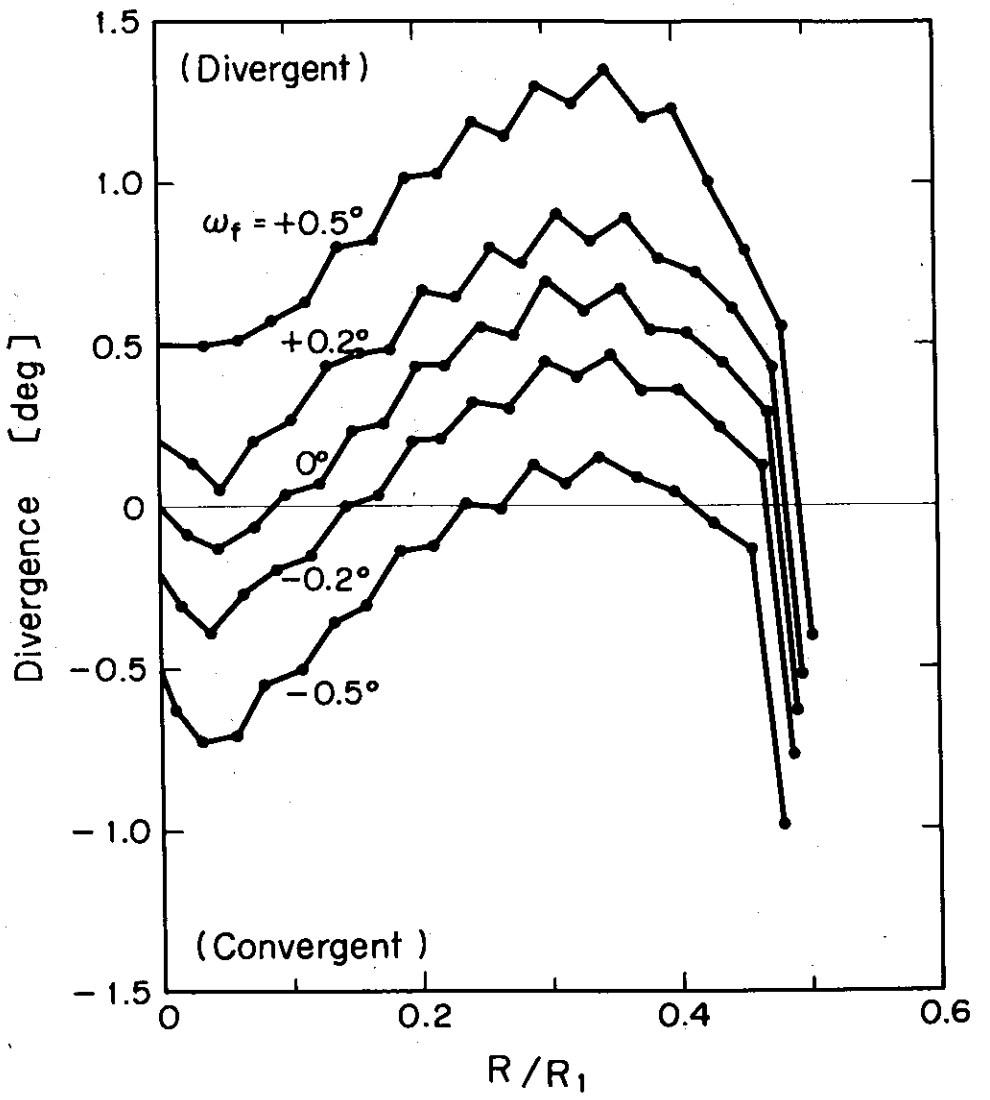

Fig. 11 Emittance diagram with the initial divergence of ω_f=0, ±0.2, ±0.5 degree for the case of f=1/3, s=1, a=0.7, G/k=1.192 (total current of 3.0A), Ψ=31.3 degree.

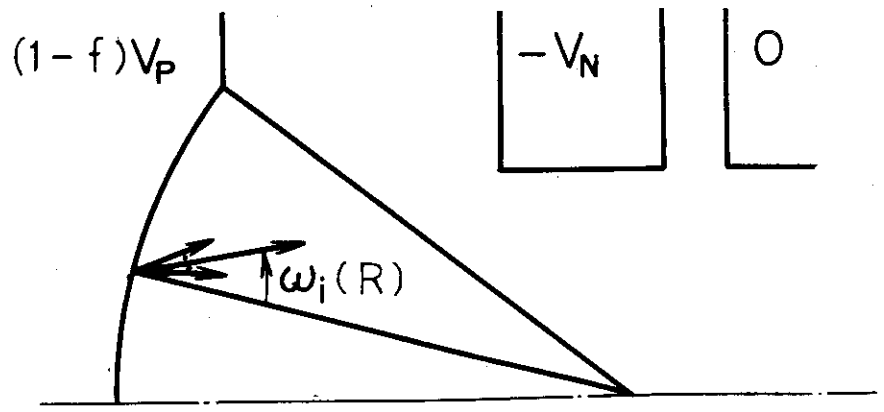

Fig. 12 Configuration where the beam is emitted in the slightly oblique direction.

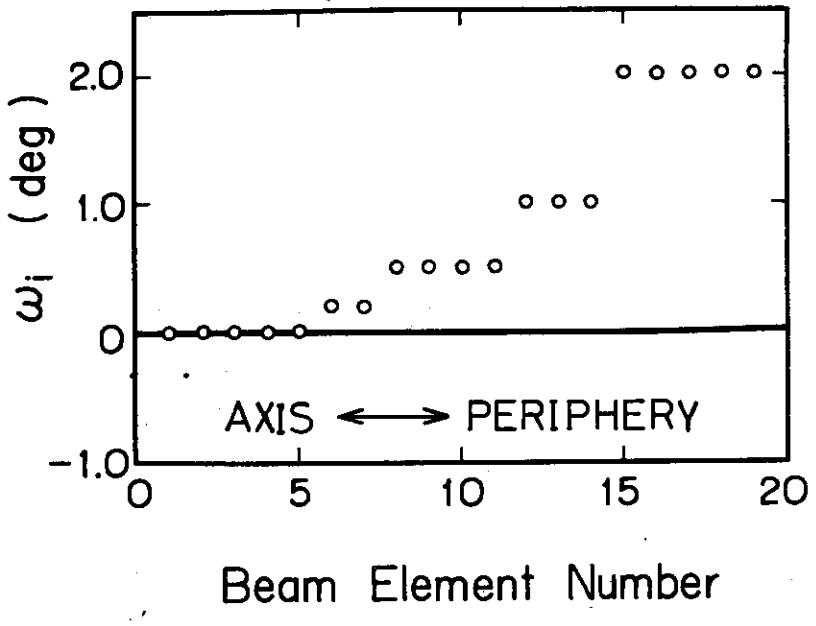

Fig. 13 One of the suitable values of ω_i versus beam element number.

Appendix I. Derivation of Eq. (7)

The equations for space-charge-limited current in one-dimensional problems are

Energy conservation law $$\frac{1}{2} Mv^2 + e\phi = \text{const} \qquad \text{(A-1)}$$

Continuity equation $$J = env = \text{const} \qquad \text{(A-2)}$$

Poisson's equation $$\frac{d^2\phi}{dx^2} = -\frac{ne}{\varepsilon_o} , \qquad \text{(A-3)}$$

where v is the velocity of ion passing through the second stage region, and n the ion density. Conbining Eqs. (A-1) and (A-2) with Eq. (A-3), we get

$$(v \frac{dv}{dx})^2 - \frac{2eJv}{\varepsilon_o M} = \text{const.} \qquad \text{(A-4)}$$

Then, the solution to Eq. (A-4) with boundary conditions $v = v_1$, $dv/dx = 0$ at $x = 0$ should satisfy the following relation.

$$(v - v_1)^{1/2}(v + 2v_1) = \frac{3}{2}\sqrt{\frac{2eJ}{\varepsilon_o M}}\, x \quad . \qquad \text{(A-5)}$$

As v is equal to v_2 at $x = d$, we get

$$(v_2 - v_1)^{1/2}(v_2 + 2v_1) = \frac{3}{2}\sqrt{\frac{2eJ}{\varepsilon_o M}}\, d \quad . \qquad \text{(A-6)}$$

On the other hand, the following relations hold.

$$k = \varepsilon_o(2e/M)^{1/2} \qquad \text{(A-7)}$$

$$\frac{1}{2} Mv_2^2 = eV \qquad \text{(A-8)}$$

$$v_1/v_2 = f^{1/2} \qquad \text{(A-9)}$$

$$G = I/V^{3/2} \qquad \text{(A-10)}$$

$$I = \pi R^2 J \qquad \text{(A-11)}$$

$$S = R/d \qquad \text{(A-12)}$$

Substituting Eqs. (A-7) $\sim$ (A-12) into Eq. (A-6), we obtain the condition that no potential hill is produced along the beam paths.

$$G/k \leq \frac{4\pi}{9} S^2(1-f^{1/2})(1+2f^{1/2})^2 \qquad \text{(A-13)}$$

Here, G/k has maximum value at $f = 1/4$. The region of G/k which satisfies above relation is shown in Fig. A-1.

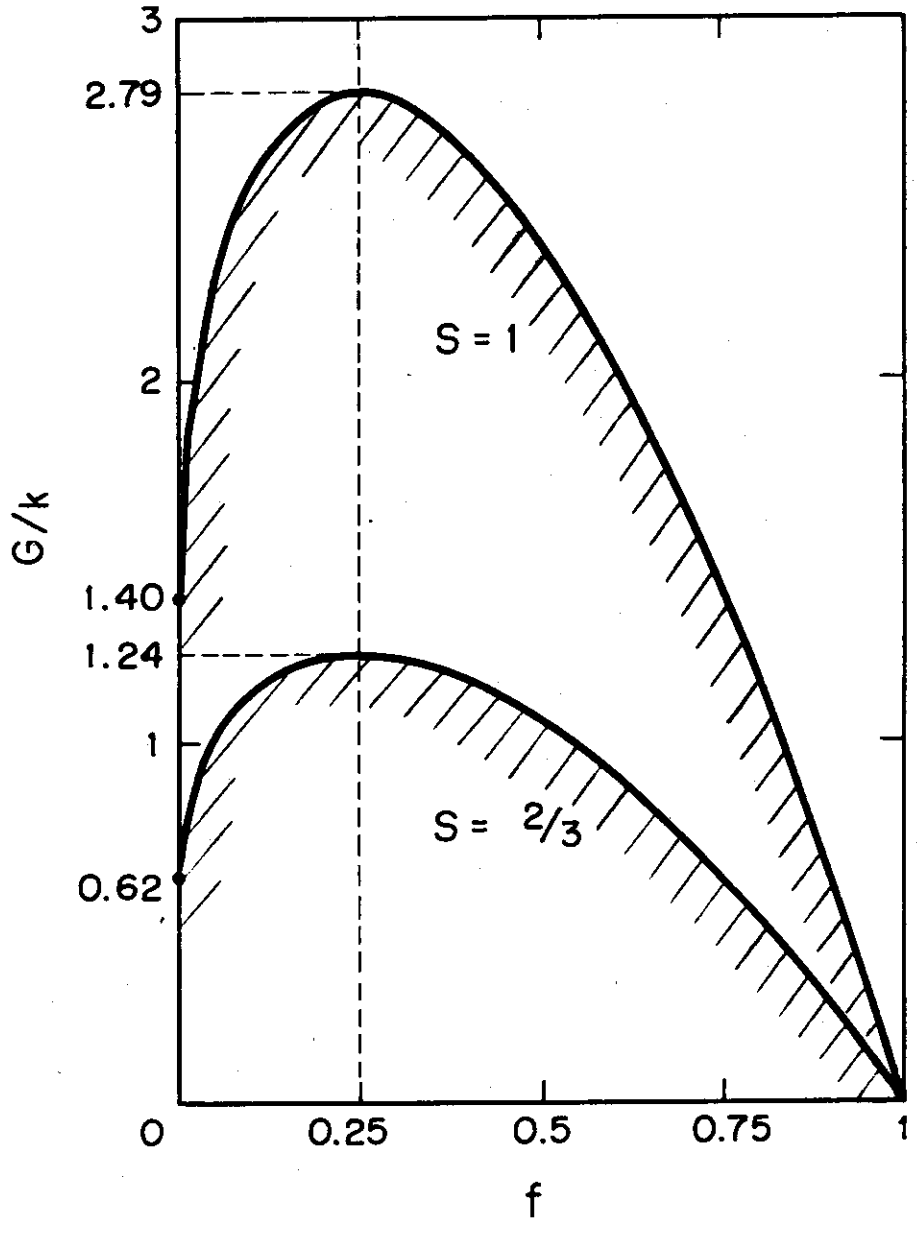

Fig. A-1 Region where no electrical potential hill is produced for s=1 and s=2/3.